Chapter 6
Three-Dimensional Imaging: A Clinically Oriented Focus

Taking advantage of the optimizations and procedures introduced in the previous two chapters, this chapter demonstrates the imaging results presently achievable at the SYRMEP beamline, with a focus closely oriented to the clinical application of propagation-based BCT.

Of note, most of the PBBCT data documented in literature to date have been limited to breast specimens featuring a small thickness [1–3]. Nonetheless, in order to demonstrate the advantages over conventional imaging, fully three-dimensional CT datasets must be produced by imaging the whole volume as done, for instance, with other phase-sensitive techniques [4–6]. In recent publications, by both the Italian and Australian collaborations [7, 8], the first full 3D reconstructions of breast specimens imaged using PB technique at clinically acceptable dose levels have been shown. In the following, based on full volume scans of three large mastectomy/lumpectomy samples, several features of PBBCT images, as 3D visualization and convenient data processing, are presented. In addition, to investigate the foreseeable diagnostic benefits associated with PBBCT, images are compared with the currently available standard clinical techniques: as a matter of fact, breast-cancer detection relies mostly on (planar) mammographic images while the intra-operative or post-surgery analysis of the resected tissue is performed by means of histological examination. In this context, two cases are compared with conventional X-ray mammography imaging and, in one case, the matching between histological and low dose PBBCT images is demonstrated. Some contents of this chapter are based on the results published in [9].

6.1 Samples and Acquisition Parameters

The work reported in this chapter was carried out following the Directive 2004/23/EC of the European Parliament and of the Council of 31 March 2004 on setting standards of quality and safety for the donation, procurement, testing, processing, preservation,

L. Brombal, *X-Ray Phase-Contrast Tomography*, Springer Theses,
https://doi.org/10.1007/978-3-030-60433-2_6

storage and distribution of human tissues. The presented images were acquired as to guide the pathologist in the lesion localization during histological preparation, according to the standard procedures of the clinic operative unit (U.C.O.) of the Anatomy and Histology Department of the University Hospital of Cattinara, Trieste. The samples were prepared from specimens of breast mastectomy and lumpectomy sent to the clinic operative unit, where they were sealed in a vacuum bag after formalin fixation. Within the energy range of interest, this process is expected not to produce substantial alterations in contrast between adipose and fibroglandular/tumoral tissue, as reported in literature [10]. Three surgical specimens containing cancer were analyzed and described by expert pathologists as follows:

- sample A is a left simple mastectomy from a 86 year old woman. The histological exam revealed a high-grade infiltrating solid carcinoma with a maximum diameter of 8 cm;
- sample B is a lumpectomy in left upper inner breast from a 84 year old woman. The histological exam revealed a moderate-grade infiltrating ductal carcinoma with a maximum diameter of 2.4 cm with a central sclerotic area;
- sample C is a right simple mastectomy from a 77 year old woman. The histological exam revealed a moderate-grade infiltrating ductal carcinoma with a maximum diameter of 9 cm.

As described in Sect. 3.5, the samples were imaged by acquiring 1200 projections in continuous rotating mode over 180°, at the maximum detector frame rate of 30 Hz. Scans were performed in 40 s, corresponding to an angular speed of 4.5 degrees/second. Due to the small vertical beam dimension (3.5 mm, FWHM), to acquire the full volume many scans (8–14) at different vertical sample positions were collected, resulting to a total scan time ranging from 5 to 9 min. By adjusting the beam intensity through planar aluminum filters (see Sect. 5.3), 5 mGy of mean glandular dose were delivered, and the specimens were imaged at 32 keV. To facilitate the comparison with results of other groups which use different dosimetric protocols [3, 8], in the following the entrance air kerma is declared for each image. Prior to reconstruction the single-material PhR was applied with $\delta/\beta = 2308$, corresponding to breast equivalent tissue.

6.2 3D BCT Reconstructions and Comparison Conventional Imaging

6.2.1 Sample A

The reconstructed three-dimensional volume of the sample A is reported in Fig. 6.1, where the three orthogonal view planes, i.e. coronal, sagittal and transverse (see inset) are displayed. In order to maintain the conventional anatomical planes, the one orthogonal to the rotation axis, usually referred to as transverse, is here identified as

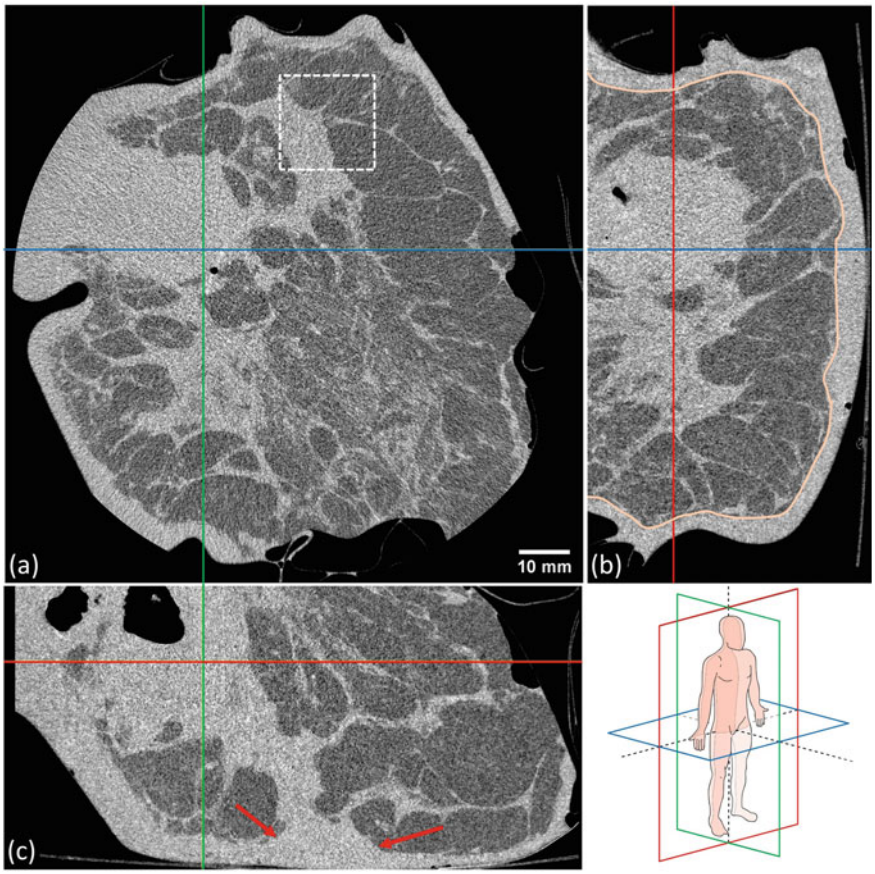

Fig. 6.1 Coronal (**a**), sagittal (**b**), transverse (**c**) views of the sample A. Line markers are centered in the bulk of the biggest tumoral focus while several accumulations of desmoplastic tissue are visible throughout the breast volume. The curved pink line in (**b**) indicates the skin margin, while the arrows in (**c**) indicate the skin involvement. The dashed square in (a) represents the crop region reported in Fig. 6.3

coronal. The sample has been scanned with an entrance air kerma of 8 mGy and its volume is approximately of 10 cm × 10 cm × 5 cm. From CT images the extension (maximum dimensions of 5 cm × 5 cm × 5 cm) and morphology of the tumor can be evaluated. Remarkably, the multiple-plane view enabled by tomography allows a clear evaluation of the various foci of the lesion, their connections and the skin involvement (see arrows in figure). These kind of features, which are cornerstones of therapeutic decision-making, are often difficult, sometimes impossible, to evaluate with standard imaging techniques.

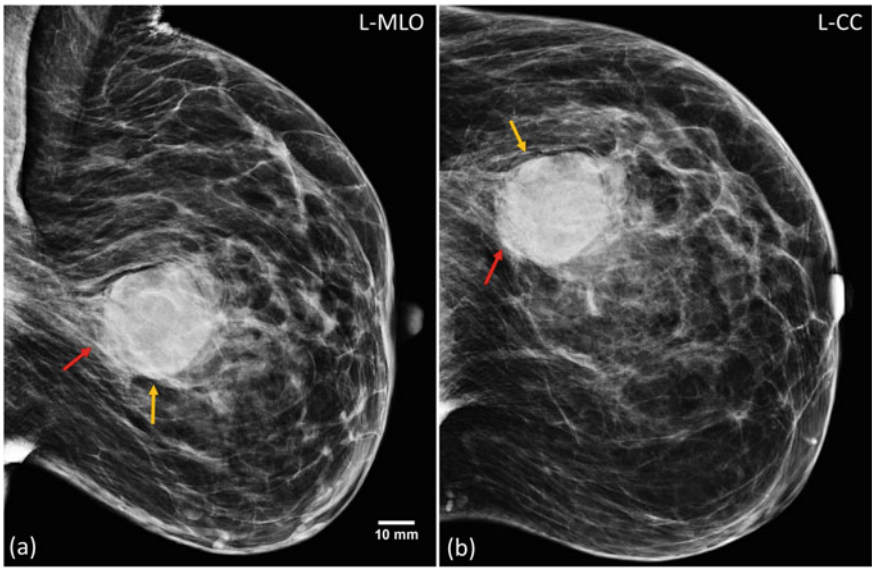

Fig. 6.2 Mammographic images of the patient before surgery corresponding to sample A: mediolateral (i.e., sagittal) view (**a**) and cranio-caudal (i.e., transverse) view (**b**). Sharp margins of the opacity are indicated by yellow arrows while shaded margins are indicated by red arrows

For comparison, Fig. 6.2 shows the mammography performed few weeks before surgery. A high-density large round opacity (diameter of 4 cm) with some lobulations, surrounded by a non-homogeneous and non-specific less dense area, can be seen. While some of its margins are sharp (yellow arrows), others are shaded and difficult to interpret (red arrows) because of tissue superposition. By comparing the images, it is clear that by avoiding tissue superposition PBBCT allows a generally more accurate morphological description of the lesion, thus leading to a higher diagnostic confidence.

Of note, from the physical perspective, is the effect of phase retrieval on the visibility of fibroglandular details: panels (a), (b) of Fig. 6.3 show a zoom of Fig. 6.1 containing a thin fibroglandular spicula reconstructed without and with phase retrieval, respectively. Considering the line profiles in panels (c), (d), the fibrous detail is clearly visible only when the phase retrieval is applied, while, in the other case, it is well below the noise level.

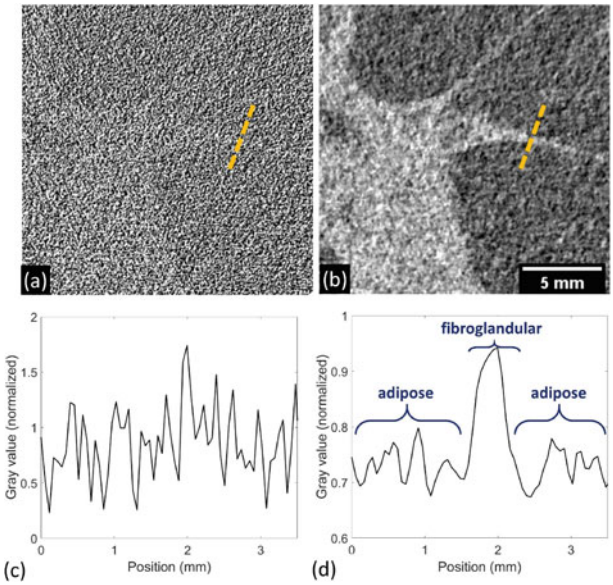

Fig. 6.3 Detail reconstructed without (**a**) and with (**b**) phase retrieval. In (**c**) and (**d**) profiles along the dashed lines of figures (**a**) and (**b**), respectively, are reported

6.2.2 Sample B

In Fig. 6.4 three orthogonal views of the sample B, acquired with an entrance air kerma of 7 mGy, are shown. The volume dimensions are 9 cm × 8 cm × 4 cm, while the crossing of line markers identifies the 2.5 cm × 2.5 cm × 2 cm tumor bulk. Surgical cuts performed during formalin fixation result in sharp interfaces between fibrous and adipose tissue and air gaps, which can be observed in the reconstruction. The tumor bulk embeds a hyper-dense sclerotic component and several microcalcifications (red circles). The irregularity of the lesion margin, as well as its spiculated appearance, are clearly visible, thus making the clinical picture compatible with a neoplastic lesion, which is confirmed by histological evaluation. Moreover, focusing on the large calcification (1.4 mm diameter) visible in the peripheral area of the sample (lower part of Fig. 6.4b), it is interesting to observe the presence of a cavity in its center, typical of benign rim calcifications.

To directly compare PBBCT and mammography, a slice oriented as the mammographic medio-lateral plane is chosen, using as a reference the aforementioned calcification, as marked by the circles in panels (a)–(c) of Fig. 6.5. It is clear that, while the mammographic image (c) represents an average of the attenuation properties of the 4 cm-thick compressed breast, the 60 μm thick CT slice (a) allows avoidance of tissue superposition. Furthermore, thanks to the three-dimensional nature of tomographic data, several processing operations other than averaging can be performed and, if needed, condensed in bi-dimensional images which are more common in breast imaging. As an example, in (b), the maximum intensity projection span-

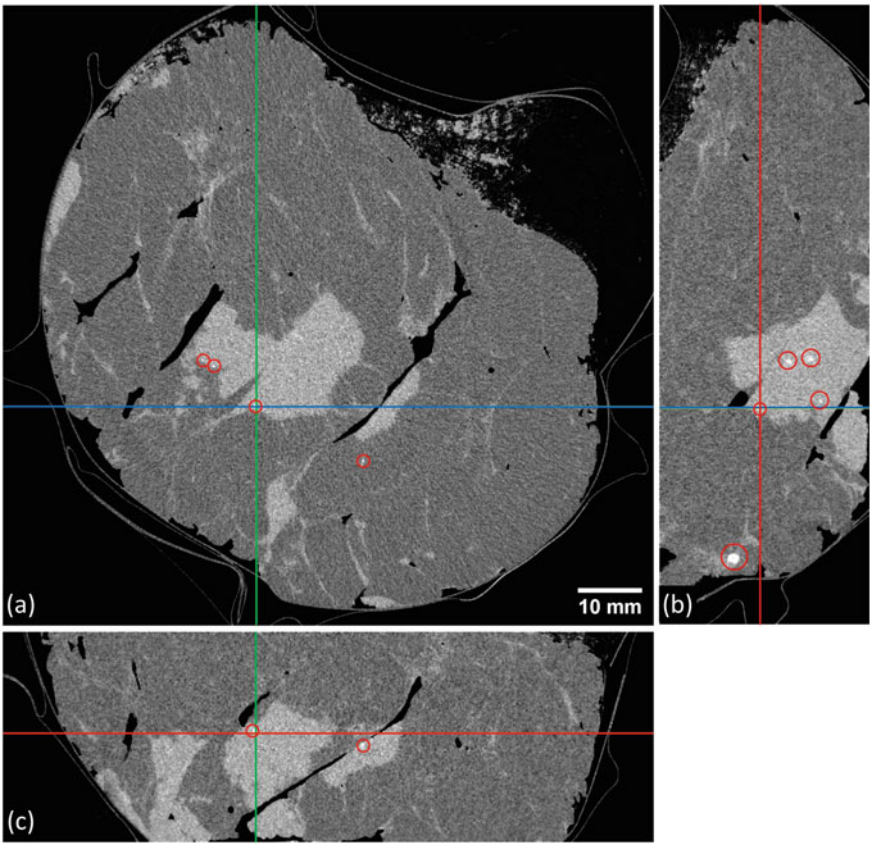

Fig. 6.4 Coronal (**a**), sagittal (**b**), transverse (**c**) views of the sample B. Line markers are centered in the bulk of the lesion, while red circles indicate microcalcifications

ning a thickness of 1.5 cm (about 300 slices) is reported. A generally good match with the mammography in terms of lesion's dimension and position is observed but, remarkably, dozens of microcalcifications in the tumor region are detected in the maximum intensity image, whereas they are missing in the mammographic examination. Moreover, following the maximum intensity projection operation, the large sclerotic component within the tumor is clearly visible (arrow in (b)).

In addition to orthogonal views display and bi-dimensional data reduction, CT images are suitable for 3D rendering as shown in Fig. 6.6. By adequately choosing the display thresholds, the fat tissue has been eliminated, fibroglandular/tumor structures have been made increasingly dark as a function of their density and the microcalcifications have been segmented (in red). The darker region within the tumor bulk encloses several calcifications and it identifies its hyper-dense sclerotic component. In general, 3D rendering has the advantage of capturing the global appearance of the lesion in terms of shape, distribution, extension and spiculation thanks to depth perception. Moreover, this kind of visualization enables further quantitative

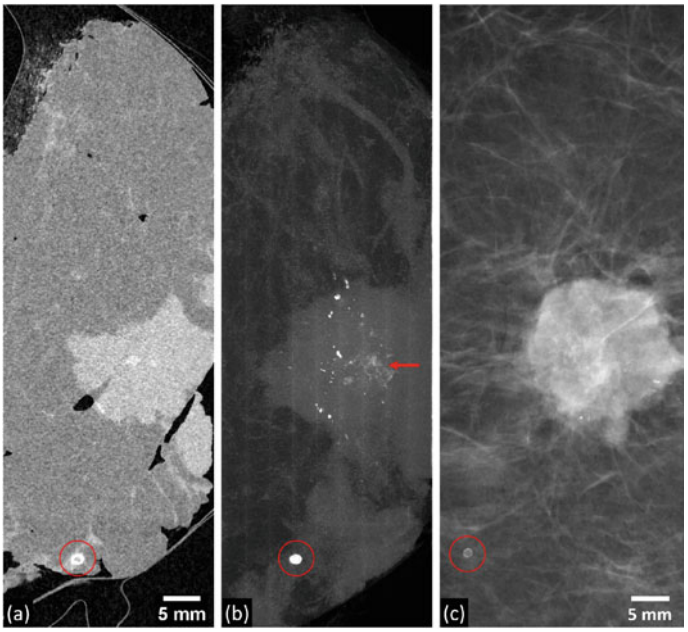

Fig. 6.5 Single slice (**a**) and maximum intensity projection (**b**) of the sagittal view of sample B. A crop of the medio-lateral pre-surgery mammographic image is reported in (**c**). Circles identify the benign rim calcification used as a reference while arrow in (**b**) indicates the hyper-dense sclerotic component

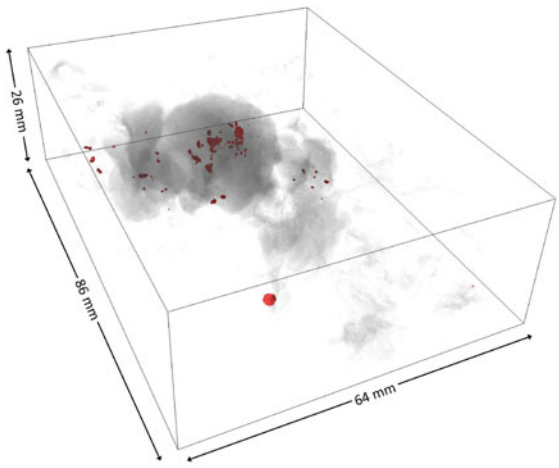

Fig. 6.6 3D rendering of the sample B. Increasingly darker regions represent fibroglandular/tumoral tissue with increasing density, red scattered volumes identify calcifications. The rendered volume is a sub-region of the whole scanned volume focusing on the lesion

analysis as, for instance, characterization of spatial and dimension distributions of microcalcifications and tumor modelling.

6.2.3 Sample C

The Sample C, of dimension 10 cm × 10 cm × 3 cm, is scanned with an entrance air kerma of 7 mGy. A multifocal lesion, marked by arrows in the image, can be seen in the coronal view displayed in panel (a) of Fig. 6.7, where the line markers are centered on a portion of it. In Fig. 6.8 a zoomed detail with dimension of 2.5 × 2.5 cm^2 obtained from the tomographic scan (a) is compared with the respective histological image (b). From the PBBCT image a lesion with well defined smooth margins (yellow line) can be clearly distinguished from a contiguous structure with irregular margins (red line). This distinction is confirmed by matching the tomographic image with the histological examination, showing an encapsulated tumor (yellow line) and separated ductal structures with papillary lesion (red line). The light green line identifies a thickened skin tissue portion which has similar shape and orientation in both

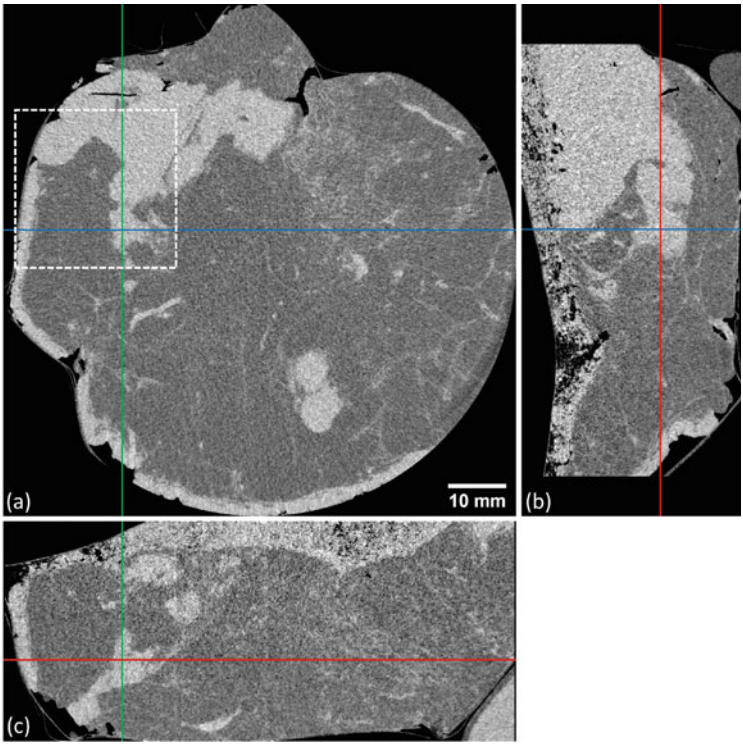

Fig. 6.7 Coronal (**a**), sagittal (**b**), transverse (**c**) views of the sample C. Line markers are centered on one portion of the largest lesion, while arrows indicate two different tumor foci. Dashed line encloses the detail shown in Fig. 6.8

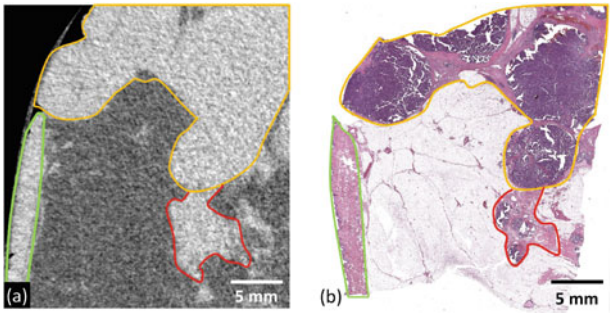

Fig. 6.8 Comparison between PBBCT (**a**) and histology (**b**). In both images, the region enclosed by the yellow line is an encapsulated lesion, the one within red line identifies ductal structures with a papillary lesion, the one within light green line is skin

PBBCT and histological images. It should be stressed that the matching between histological images and radiological images (with low radiation dose) is peculiar of the proposed PBBCT system. In fact, tissue superposition is encountered both in mammography and in tomosynthesis imaging, whereas insufficient spatial resolution generally affects other 3D techniques (e.g., MRI and ultrasound).

6.2.4 Future Developments

As demonstrated in Sect. 5.1, the propagation distance plays a crucial role in terms of image quality in PB configuration. Specifically, the SNR increase associated with the phase-retrieval is found to have, as a first approximation, a linear dependence with the propagation distance. As previously detailed, in light of these findings an extension will be installed at the SYRMEP beamline, enabling to reach patient-to-detector distances up to about 4.5 m. This upgrade is expected to improve the SNR by approximately a factor of two, even when both the small changes in magnification due to larger distance (from 1.05 at 1.6 m to 1.17 at 4.5 m) and the flux reduction (about 10% at 32 keV) due to the increased air attenuation are taken into account. To give an idea of the foreseen impact of the upgrade on image quality, sample C has been scanned with an exposure yielding a 2-fold higher SNR (i.e., 4-fold higher dose, 20 mGy MGD_t) and the results have been compared with the present 5 mGy image reference, as shown in Fig. 6.9. By zooming on a detail enclosing the margins of the main lesion (panels (c), (d)), it is clear that increasing the SNR by a factor of 2 allows to determine the presence of spiculae and thin connections of fibroglandular/tumoral tissue (green arrows), which are missed in the reference image (red arrows). Although the actual impact of the beamline upgrade should be assessed thorough dedicated measurements following its implementation, these results clarify the clinical impact of the upgrade, adding to the theoretical and quantitative demonstrations provided in Chap. 5.

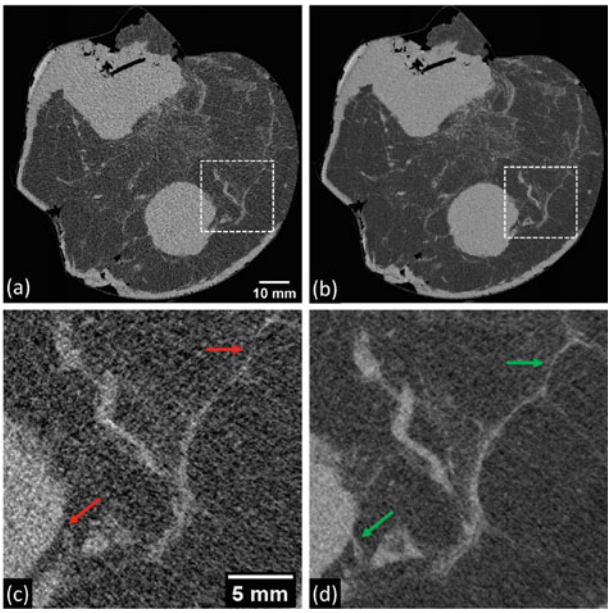

Fig. 6.9 Slice of the sample C scanned at MGD_t of 5 mGy and SNR = 9.1 (**a**), 20 mGy and SNR = 18.8 (**b**), mimicking a 5 mGy acquisition at the upgraded SYRMEP beamline. In (**c**–**d**) a zoom of a detail of (**a**), (**b**), as shown by the dashed line, is reported. Arrows point toward thin connections of fibroglandular tissue which are not visible in (**c**, red) and visible in (**d**, green). SNR is measured within the spheroidal hyper-dense mass

Along with the optimization of physical parameters such as the propagation distance, the use and/or development of ad-hoc reconstruction algorithms is a powerful tool to improve image quality, especially SNR, at a constant radiation dose. Albeit the presented images are reconstructed through the filtered-back-projection, which is arguably the most standard and widely used algorithm, the use of iterative reconstruction algorithms has demonstrated to provide convincing results [11]. In particular, the SYRMA-3D collaboration is developing a dedicated SART algorithm [12] making use of a 3D bilateral filter as a regularization factor during the iterative process [13, 14]. This algorithm, featuring several tunable parameters, has the advantage to allow for specific optimization on BCT images. Despite this optimization is still in progress, the beneficial effects of this algorithm are qualitatively shown in Fig. 6.10, displaying a section of sample C reconstructed with FBP (a) and SART (b) at 5 mGy of dose level. The use of dedicated SART reconstruction yields a SNR improvement of 40% (measured within the spheroidal lesion), while no evident degradation of spatial resolution is observed, as visible in the detail in panels (c), (d).

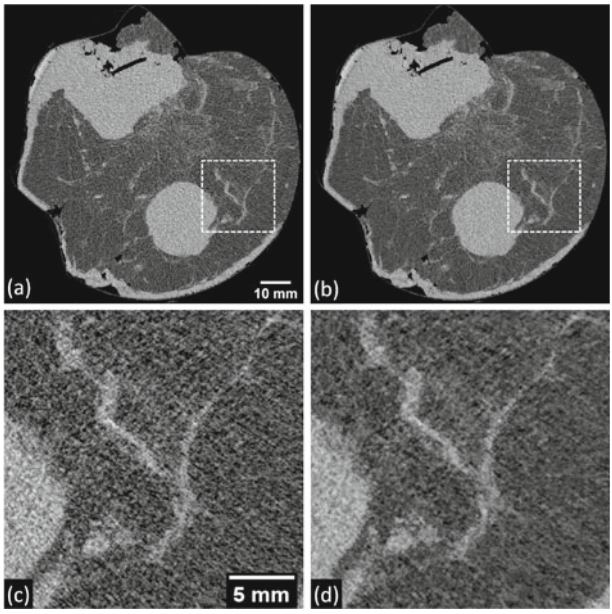

Fig. 6.10 Slice of the sample C reconstructed via FPB (**a**) and ad-hoc SART (**b**) algorithms. In (**c**), (**d**) a zoomed detail of (**a**), (**b**). as indicated by the dashed line, is shown. SNR measured within the spheroidal mass is 9.1 in (**a**) and 12.8 in (**b**)

6.3 Remarks Towards the Clinics

The images shown in this chapter represent an important step forward in the clinical implementation of phase-contrast breast CT at Elettra. The comparison between tomographic scans and standard mammographic images demonstrates that the 3D nature of tomographic data allows to avoid tissue superposition, while the high spatial and contrast resolutions determine a more accurate morphological description of neoplastic lesions. Clinically relevant conclusions on the malignant/benign nature, invasiveness and grading of a neoplastic lesion can be drawn from the detailed characterization of its volume, shape, margins, number and morphology of calcifications offered by PBBCT.

At present, digital breast tomosynthesis (DBT) is also envisaged as a tool to tackle issues as detection of microcalcifications and reduction of tissue superposition effects [15]. In fact, DBT is an emerging technology providing pseudo-3D reconstructions of the breast through the acquisition of multiple projections over a limited angular span. To better investigate its effectiveness in breast cancer screening and diagnosis, several DBT-based clinical trials are underway, but the reports regarding its capabilities in microcalcification detection are still mixed [16, 17]. In any case, diffrently from BCT which is a fully three dimensional technique, DBT offers pseudo-3D information, e.g., not allowing operations such as re-slicing in other view planes. Conversely, the possibility offered by CT of concentrating three-dimensional features in bi-dimensional images may be appealing to radiologists used to planar or

quasi-planar mammographic techniques. As in the example shown in the previous section, the presence of hyper-dense structures and calcifications can be highlighted in a single image through maximum intensity operations, providing higher sensitivity if compared with conventional radiology. Moreover, being monochromatic CT inherently quantitative, the collected images can be used to characterize breast tissues in terms of absolute attenuation coefficients as shown, for instance, in [18]. The availability of high-resolution tomographic datasets also paves the way for 3D rendering and segmentation. This would be beneficial in evaluating spatial distribution of lesions and microcalcifications, and would serve as a reference for the surgeon in the pre-operative planning stage. Considering that PBBCT images can be matched to histological images even at low (i.e. clinically acceptable) radiation dose, their use in a clinical setting would allow for a more accurate tumor grading (TNM classification), where a precise assessment of lesion's dimensions is crucial. As in the case of specimens shown in this chapter, CT images can also serve as a guide in the specimen cutting process in pathological examination.

Focusing on clinical implementation, the exam duration is still a concern that needs addressing: to ensure patient comfort and to reduce motion-related artifacts, it should be kept as short as possible. To this end, the introduction of the flattening filter described in Sect. 5.3 would increase the usable vertical dimension of the beam (from 3.5 mm to $\gtrsim$ 5 mm), leading to a 40% (or higher) reduction of the scan time. Concurrently, the possibility of reducing the number of projections along with the use of iterative reconstruction algorithms, as recently reported by [11], would further reduce the scan time by 20–30%, yet maintaining a comparable image quality. The combined effect of these improvements will bring to reduction of more than 50% in the overall exam duration.

References

1. Pacilè S, Brun F, Dullin C, Nesterets Y, Dreossi D, Mohammadi S, Tonutti M, Stacul F, Lockie D, Zanconati F et al (2015) Clinical application of low-dose phase contrast breast CT: methods for the optimization of the reconstruction workflow. Biomed Opt Express 6(8):3099–3112. https://doi.org/10.1364/BOE.6.003099
2. Longo R, Arfelli F, Bellazzini R, Bottigli U, Brez A, Brun F, Brunetti A, Delogu P, Di Lillo F, Dreossi D et al (2016) Towards breast tomography with synchrotron radiation at elettra: first images. Phys Med Biol 61(4):1634. https://doi.org/10.1088/0031-9155/61/4/1634
3. Baran P, Pacile S, Nesterets Y, Mayo S, Dullin C, Dreossi D, Arfelli F, Thompson D, Lockie D, McCormack M et al (2017) Optimization of propagation-based X-ray phase-contrast tomography for breast cancer imaging. Phys Med Biol 62(6):2315. https://doi.org/10.1088/1361-6560/aa5d3d
4. Keyrilainen J, Fernández M, Karjalainen-Lindsberg M-L, Virkkunen P, Leidenius M, Von Smitten K, Sipila P, Fiedler S, Suhonen H, Suortti P et al (2008) Toward high-contrast breast CT at low radiation dose. Radiology 249(1):321–327. https://doi.org/10.1148/radiol.2491072129
5. Zhao Y, Brun E, Coan P, Huang Z, Sztrókay A, Diemoz PC, Liebhardt S, Mittone A, Gasilov S, Miao J et al (2012) High-resolution, low-dose phase contrast X-ray tomography for 3d diagnosis of human breast cancers. Proc Natl Acad Sci 109(45):18290–18294. https://doi.org/10.1073/pnas.1204460109

6. Brun E, Grandl S, Sztrókay-Gaul A, Barbone G, Mittone A, Gasilov S, Bravin A, Coan P (2014) Breast tumor segmentation in high resolution X-ray phase contrast analyzer based computed tomography. Med Phys 41(11):111902. https://doi.org/10.1118/1.4896124
7. Brombal L, Golosio B, Arfelli F, Bonazza D, Contillo A, Delogu P, Donato S, Mettivier G, Oliva P, Rigon L et al (2018c) Monochromatic breast computed tomography with synchrotron radiation: phase-contrast and phase-retrieved image comparison and full-volume reconstruction. J Med Imaging 6(3):031402. https://doi.org/10.1117/1.JMI.6.3.031402
8. Pacilè S, Baran P, Dullin C, Dimmock M, Lockie D, Missbach-Guntner J, Quiney H, McCormack M, Mayo S, Thompson D et al (2018) Advantages of breast cancer visualization and characterization using synchrotron radiation phase-contrast tomography. J Synchrotron Radiat 25(5). https://doi.org/10.1107/S1600577518010172
9. Longo R, Arfelli F, Bonazza D, Bottigli U, Brombal L, Contillo A, Cova M, Delogu P, Di Lillo F, Di Trapani V et al (2019) Advancements towards the implementation of clinical phase-contrast breast computed tomography at elettra. J Synchrotron Radiat 26(4). https://doi.org/10.1107/S1600577519005502
10. Chen R, Longo R, Rigon L, Zanconati F, De Pellegrin A, Arfelli F, Dreossi D, Menk R, Vallazza E, Xiao T et al (2010) Measurement of the linear attenuation coefficients of breast tissues by synchrotron radiation computed tomography. Phys Med Biol 55(17):4993. https://doi.org/10.1088/0031-9155/55/17/008
11. Donato S, Brombal L, Tromba G, Longo R et al (2018) Phase-contrast breast-CT: optimization of experimental parameters and reconstruction algorithms. In: World congress on medical physics and biomedical engineering 2018. Springer, pp 109–115. https://doi.org/10.1007/978-981-10-9035-6_20
12. Kak AC, Slaney M, Wang G (2002) Principles of computerized tomographic imaging. Med Phys 29(1):107–107. https://doi.org/10.1118/1.1455742
13. Golosio B, Brunetti A, Cesareo R (2004) Algorithmic techniques for quantitative compton tomography. Nucl Instrum Methods Phys Res Sect B Beam Interact Mater Atoms 213:108–111. https://doi.org/10.1016/S0168-583X(03)01542-8
14. Oliva P, Golosio B, Arfelli F, Delogu P, Di Lillo F, Dreossi D, Fanti V, Fardin L, Fedon C, Mettivier G et al (2017) Quantitative evaluation of breast CT reconstruction by means of figures of merit based on similarity metrics. In: 2017 IEEE nuclear science symposium and medical imaging conference (NSS/MIC). IEEE, pp 1–5. https://doi.org/10.1109/NSSMIC.2017.8532786
15. Sechopoulos I (2013) A review of breast tomosynthesis. Part I, the image acquisition process. Med Phys 40(1). https://doi.org/10.1118/1.4770279
16. Marinovich ML, Hunter KE, Macaskill P, Houssami N (2018) Breast cancer screening using tomosynthesis or mammography: a meta-analysis of cancer detection and recall. JNCI J Natl Cancer Instit 110(9):942–949. https://doi.org/10.1093/jnci/djy121
17. Choi JS, Han B-K, Ko EY, Kim GR, Ko ES, Park KW (2019) Comparison of synthetic and digital mammography with digital breast tomosynthesis or alone for the detection and classification of microcalcifications. Eur Radiol 29(1):319–329. ISSN 1432-1084. https://doi.org/10.1007/s00330-018-5585-x
18. Piai A, Contillo A, Arfelli F, Bonazza D, Brombal L, Cova MA, Delogu P, Trapani VD, Donato S, Golosio B, Mettivier G, Oliva P, Rigon L, Taibi A, Tonutti M, Tromba G, Zanconati F, Longo R (2019) Quantitative characterization of breast tissues with dedicated CT imaging. Phys Med Biol 64(15):155011. https://doi.org/10.1088/1361-6560/ab2c29